

RESEARCH ARTICLE | AUGUST 24 2022

Investigating the link between LeTID and hydrogen induced contact resistance in PERC devices

Donghao Liu; Mohsen Goodarzi; Joshua Deru; Peter R. Wilshaw; Phillip Hamer; Ruy Sebastian Bonilla ✉



AIP Conf. Proc. 2487, 130008 (2022)

<https://doi.org/10.1063/5.0089337>



Export
Citation

CrossMark

Articles You May Be Interested In

LeTID in HPMC-Si wafers studied by hyperspectral photoluminescence imaging

AIP Conference Proceedings (August 2022)

Low-T anneal as cure for LeTID in Mc-Si PERC cells

AIP Conference Proceedings (August 2019)

Suppression of LeTID in p-type multi-crystalline PERC silicon solar cells by biased annealing process

AIP Conference Proceedings (August 2022)

500 kHz or 8.5 GHz?
And all the ranges in between.

Lock-in Amplifiers for your periodic signal measurements



Find out more



Investigating the Link between LeTID and Hydrogen Induced Contact Resistance in PERC devices

Donghao Liu¹, Mohsen Goodarzi¹, Joshua Deru¹, Peter R. Wilshaw¹ Phillip Hamer², and Ruy Sebastian Bonilla^{1, a)}

¹*Department of materials, University of Oxford, Oxford, OX1 3PH, United Kingdom*

²*School of Photovoltaic and Renewable Energy Engineering, University of New South Wales, Sydney, NSW, 2052, Australia*

^{a)} Corresponding author: sebastian.bonilla@materials.ox.ac.uk

Abstract. In recent years academia and industry have made significant efforts to mitigate the problem of LeTID in silicon solar cells, particularly in p-type multi crystalline PERC cells. Many of these approaches involve a post-firing thermal anneal between 300-500 °C after metal contact firing. This paper investigates observed increases in the front contact resistance of PERC cells in this temperature range. Changes in contact resistance have been primarily attributed to a hydrogen passivation effect, which might then be used to observe and study hydrogen kinetics. A new sample structure is developed to allow a more direct measurement of the current-voltage characteristics of the front contacts, without the contribution from resistance elsewhere in the cell. A careful analysis of such measurements leads to three key findings: (i) It is experimentally shown that there is no increase in resistance for any region of the device other than the front contact. (ii) It is shown that the contact resistance change is affected by the frequency of in-situ measurements and becomes highly unstable once resistance change reaches a high value, and (iii) Annealing prior I-V measurements can act to significantly increase the rate at which contact resistance changes, likely through an increase in the mobile hydrogen concentration throughout the cell. These findings are crucial to the understanding and future study of hydrogen in silicon and its relation to degradation in solar cells.

INTRODUCTION

Degradations in silicon solar cells have been observed in industrial [1] and research settings [2][3] for decades. Studying the mechanism of degradations and finding techniques to mitigate them are essential to maintain the cell's efficiency and boost the deployment of photovoltaic solar energy. Silicon solar cells are susceptible to various types of degradations: adhesion loss between encapsulants and other layers, corrosion of solder joints, and degradations in the electrical performance of the semiconductors. These mechanisms are induced both by the manufacturing processes and the in-field operation [4-7]. Light induced degradation is one of the main types of electrical performance degradation induced by the in-field operation. It is caused by the increase in excess minority carrier recombination under illumination or by forward biasing current [8-10]. Initial observations of light induced degradation in p-type CZ devices were found to be the result of the formation of boron-oxygen complexes [8]. However, Ramspeck et al. [11] and Fertig et al. [12] reported that a strong light induced degradation in efficiency as high as 5 % rel could occur at 75 °C after dark annealing in multi-crystalline silicon solar cells. Such degradation could not be explained by the previous Boron-related model. The degradation was later referred to as Light and Elevated Temperature Degradation (LeTID). LeTID was found to cause the conversion efficiency to decrease by over 10% relative, especially for silicon solar cells with dielectric passivated surfaces on both sides [11]. It has been reported that LeTID affect all types of silicon solar cells including p-type (B-doped and Ga-doped) and n-type silicon, but LeTID in p-type multi PERC is much more significant than that of other materials [3, 13]. To date, no final explanation has been reported for the mechanism of LeTID, yet it is essential to find suitable and efficient technique to mitigate its effects.

Although the mechanisms behind LeTID are still not clear, it has been reported that annealing after metal contacts firing is highly effective to reduce LeTID and recover the minority carrier lifetime of silicon specimens [14]. However, this process results in a dramatic reduction in cell's fill factor, which has been linked to an undesirable increase in contact resistance originating from the front contact [14, 15]. Peral et al. [16] concluded that the increase of contact resistance was likely caused by the thickening of glass layer surrounding silver crystallites at the silver-silicon interface. Later Chan et al. [17] and Hamer et al. [18] reported that an applied electric bias altered the change of contact resistance recorded by in-situ current-voltage measurements. Therefore, it can be speculated that the change of contact resistance could be caused by a charged species that responds to the change in the internal electric field of the cell. These findings indicated that increases in contact resistance could be linked to the LeTID root causes, and therefore related to mobile charged species inside the silicon cell, most likely hydrogen.

Hydrogen plays important role in PV industry and has been used in defects passivation process as a well-established technique to increase lifetime [19, 20]. $\text{SiN}_x\text{:H}$ and $\text{AlO}_x\text{:H}$ dielectric layers are the main dielectrics used in the passivated emitter and rear cell (PERC) devices, and act as hydrogen sources during firing [21, 22]. Kester et al. [23] showed that LeTID was only observed for silicon solar cells fired with dielectric layers containing hydrogen. Vargas et al. [24] used Fourier transform infrared spectroscopy (FTIR) to demonstrate the correlation between the hydrogen released from SiN_x layer and the extent of the degradation. Hamer et al. [25] showed that the change of resistance at elevated temperature can be controlled by the bias applied to the cell. Therefore, it has been hypothesised that the increase of resistance should be related to hydrogen in silicon solar cells and hydrogen could be involved in the LeTID of silicon solar cells in the field. Hence, the link between LeTID and Hydrogen Induced Contact Resistance (HICR) in PERC devices is investigated here.

EXPERIMENTAL

Specimen Preparation

Standard commercial full-size p-type boron-doped mono crystalline PERC cells from different manufacturers were used in this work. The cells were then cleaved into $1.5 \times 2 \text{ cm}^2$ samples for further processing. While Hamer et al. [25] have shown that the front contact resistance increases during post-firing thermal processes, it has not been established whether this resistance change is only originating from the silver-silicon interface, or if it also includes the emitter or junction. Previous studies have measured series resistance between the front and rear contacts of PERC cell structures by in-situ IV curves. To observe more accurately what is occurring at the interface, it is desirable to develop a new measurement approach that avoids interference from the p-n junction or the rear contact. In this work, we designed and created a new geometry of sample to enable us to measure different components of series resistance separately. The new sample geometry is shown in FIGURE 1. Photoresist is painted to cover one silver finger and a small portion of busbar, while back aluminium contact is fully covered by photoresist. Samples are left to dry overnight. A nitric acid and DI water solution, 2:3 ratio by volume, is used to etch off the remaining silver. A photoresist layer is painted on top of the existing photoresist line to isolate silver finger with a larger area, and a circular line of photoresist is drawn around the photoresist coated region, as depicted in FIGURE 1. Then, specimens are left to dry for ~30 minutes. Reactive Ion Etching (RIE) is then used to remove the nitride layer with 25 sccm CHF_3 and 25 sccm Ar for ~10 minutes. 100 nm aluminium is deposited on the front surface using a thermal evaporator. Acetone combined with ultrasonic bath is then used to etch off the remaining photoresist to expose the front Ag contact. Through this process the new geometry of specimen is generated including an Al front contact.

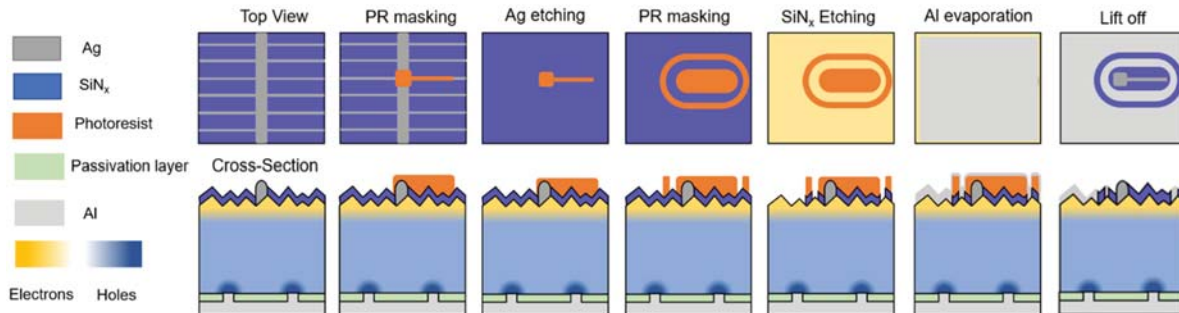


FIGURE 1. Schematic of the modified geometry process for PERC specimen

Current-voltage Measurement Set Up

A closed-loop controlled hot plate is used to heat the sample in a dark box. A mechanically affixed thermocouple and PID controller are used to adjust desired temperatures on an aluminium sample stage. A Keithley 2401 source measuring unit (SMU 1) is used for in-situ observation of I-V characteristics for the sample, while a second Keithley 2601 source measuring unit (SMU 2) is used to apply external bias to samples. I-V characterization was performed before and during annealing. With control of heating temperature, external applied bias, and measurement frequency, we were able to produce different experimental conditions that led to changes of contact resistance. FIGURE 2 (a) illustrates the previous geometry and measurement set up used to measure series resistance on original PERC cell received from manufactures. Such a geometry measures a string resistance including front and rear contacts, as well as resistance inside the device structure. In this work, we suggest a new geometry depicted FIGURE 2 (b) that modified the original cells to enable measuring different components of series resistance separately. FIGURE 2 (b) shows a schematic of the measurement set up with the second direct aluminium front contact to the emitter. As can be seen in both the regular and new measurement set ups, an external source is used to apply desired bias to the junction during annealing step. The bias source is then turned off during the I-V measurements, such that the I-V measurement SMU is the only source impacting charge carriers inside the samples. With this set up we were also able to evaluate the effects that the frequency of measurement have in the charge carriers' behaviour, and consequently the changes and instabilities in the measured resistance.

Contact resistance changes at any specific time were calculated from the difference between the measured resistance at that time and the initial measured resistance at elevated temperature before the measurements started. Initially, four sets of measurements were performed to obtain the resistance change between (i) the Ag finger and the rear Al contact in the unmodified specimen, (ii) the Ag finger and the rear Al contact of modified specimen, (iii) the Ag finger and the new Al front contact of a modified specimen, and (iv) the front Al and the rear Al contacts of modified specimen. These four resistance paths as shown in FIGURE 2. Unmodified and modified samples were measured at 400° C for 180 minutes with external forward and reverse ($\pm 0.5V$) biases applied continuously for 30 min intervals. Different measurement frequencies were also used in this in-situ IV set up to study the impact of the measurement itself on changes in contact resistance. Samples were measured 60 times at 20, 60 and 180 seconds time intervals at 400° C, with external forward and reverse ($\pm 0.5A$) bias through SMU 2 between measurements. Finally, different pre-annealing treatments were performed on samples to study the impact of time at elevated temperature on changes in front contact resistance. All pre-annealing treatments were performed when samples were under 2.5 V reverse bias at different temperatures, and for different durations. A set of samples were pre-annealed for 2 hours at different temperatures ranging from 325 to 400 °C while another set of samples were pre-annealed at 400 °C for different duration between 0 and 22 hours. This allowed separation of the effects of temperature and time.

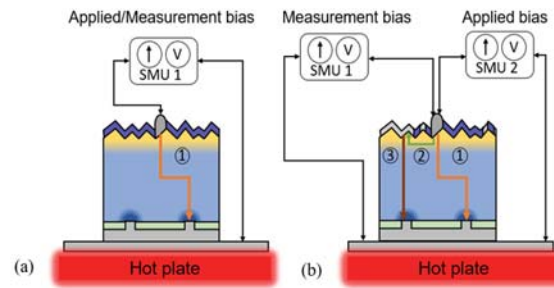


FIGURE 2. Schematic of measurement model for samples with different geometry. (a) Old geometry and circuit: ① Measurement from front Ag to rear contact. (b) Modified geometry and circuit: ① Measurement from front Ag to rear contact ② Measurement from front Ag to front Al ③ Measurement from front Al to rear contact

RESULTS AND DISCUSSION

Origin of the Series Resistance Increase

Results of unmodified and modified samples (a and b in FIGURE 2) measured at 400° C with forward and reverse ($\pm 0.5V$) biases applied are shown in FIGURE 3. ΔR_c saturates around 100 Ω after 150 min with forward bias, while

reverse bias suppresses ΔR_c from its forward bias values immediately but not to the initial value, in line with results from previous work [25]. FIGURE 3 (b) shows ΔR_c of path 1 in FIGURE 2 (b) for the modified specimen, which shows a similar trend as that shown in FIGURE 3 (a), suggesting that no artefacts were introduced with the specimen modification. It should be noted, however, that ΔR_c in the first bias cycle is 10 times larger in the modified structure (b) than in the unmodified one (a). The final saturated ΔR_c value in the reversed bias condition is also found much larger. This requires further investigation in order to isolate the mechanisms behind the saturation in ΔR_c . FIGURE 3 (c) shows the resistance change between the Ag finger and the front Al. Again the resistance along this path demonstrated a very similar trend of resistance change as that shown in FIGURE 3 (a). Such similar patterns in resistance changes suggests the same mechanisms are in fact behind these changes. The resistance change between the front Al and back Al, however, is negligible as it is shown in FIGURE 3 (d) and are approximately two orders of magnitude lower than the changes in paths including silver front contact. These results demonstrate that there are no significant changes in either the bulk or rear contact resistance during annealing, and that the increase in series resistance is solely due to the Ag/Si interface.

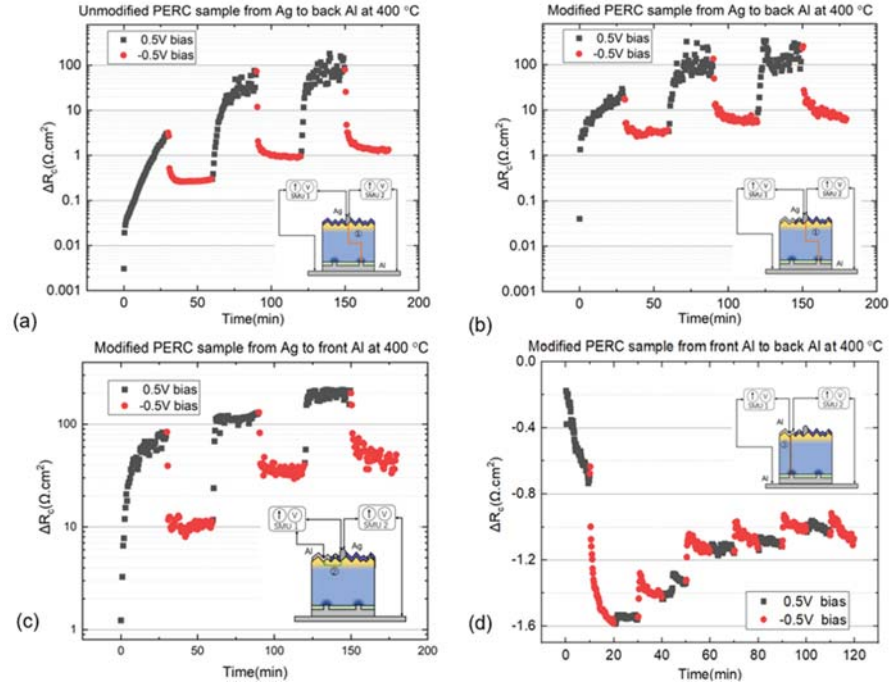


FIGURE 3. Test results of previous path and new path of modified and unmodified specimen. (a) ΔR_c as a function of annealing time and applied bias between the Ag and rear Al contacts for the unmodified specimen, $R_{c \text{ initial front Ag-back Al}} = 0.2 \Omega \cdot \text{cm}$.

(b) ΔR_c as a function of annealing time and applied bias between the Ag and rear Al contacts for the modified specimen, $R_{c \text{ initial front Ag-back Al}} = 1.3 \Omega \cdot \text{cm}$. (c) ΔR_c as a function of annealing time and applied bias between the Ag and front Al contacts for the modified specimen, $R_{c \text{ initial front Ag-front Al}} = 4.7 \Omega \cdot \text{cm}$. (4) ΔR_c as a function of annealing time and applied bias between the front Al and rear Al contacts for the modified specimen, $R_{c \text{ initial front Al-back Al}} = 2.9 \Omega \cdot \text{cm}$.

Influence of Measurement Frequency

In our prior work the number of I-V measurements recorded over the biasing interval was kept constant to enable direct comparison across samples [25]. Since the applied bias has been directly linked to the change in resistance, in this work we tested the potential effect that the frequency of I-V measurements and the duration of bias can have on contact resistance and its change rate. FIGURE 4 (a) shows ΔR_c with fixed number of measurements in forward and reverse bias, using 20, 60 and 180 s time intervals between measurements, resulting in 3 different bias durations. The results show that both the rate at which contact resistance changes and the final saturated value are highly depended on bias saturation and measurement frequency. The sample measured every 20 s saturated around 100 Ω after 250 min measurement, while the sample measured every 180 s only reached around 2 Ω after 400 min measurement. It is also important to note that once ΔR_c exceeds $\sim 20 \Omega$, it becomes highly unstable, as observed for the specimen measured

every 20 s for longer than 200 minutes. However, as FIGURE 4 (b) shows ΔR_c for specimens from different manufacturer, keeping the bias duration constant and only changing the measurements time intervals had minimal impact on the final saturated ΔR_c , but, insignificant affects on the rate at which ΔR_c . Some differences were recorded on the rate at which ΔR_c decreases under reverse bias. The specimen measured every 20 s still has highest rate of ΔR_c , while specimen measure every 60 s and 180 s have approximately the same $\Delta R_c/dt$. Considering the link between LeTID and HICR we speculate that the differences observed in different specimens may originate from differences in H concentration, or changes in the Ag-Si interface morphology of each specimen. These results would hence show that the manufacturing conditions are of importance for the final H concentration, yet further investigation are required to isolate the underlying mechanisms This is in agreement with the investigations of LeTID [26].

To explain the change in front contact resistance as well as the impact of the measurement frequency, the field at the contact itself should be considered. When metal contacts a semiconductor, it produces a Schottky barrier contact with a high concentration of interface states. It is hypothesized that hydrogen passivates these states and leads to increase of Schottky barrier height, and therefore the increase in resistance. The Schottky barrier also acts as an obstacle for H- to occupy these interface states. Therefore, when the fixed forward bias is removed and a measurement taken, barrier height would be reduced a small amount giving H the possibility to occupy interface states, which in turn reduces Fermi level pinning and increases barrier height. The increases in measurement frequency can hence cause increase of resistance change rate and higher saturated resistance. The observed instability is also related to the field across the contact.

Once the contact resistance increases sufficiently and there is substantial Schottky barrier height, it becomes possible for a bias, either fixed or swept due to measurement, to generate extremely large fields, which may lead to breakdown occurring. This hypothesis requires further investigation and experimental confirmation. As mentioned in the previous section and shown in FIGURE 2, the biasing source SMU2 was turned off during the measurements. Thus, SMU1 which is used for I-V characterization is the only source that impacts mobile charges carriers inside the structure. Hence, the frequency at which the measurements are performed has great impact on the contact resistance change. Higher measurement frequency causes higher contact resistance change rate and higher saturated resistance, which could be related to the amount of metal-semiconductor interface sates occupied by the hydrogen from silicon bulk during annealing.

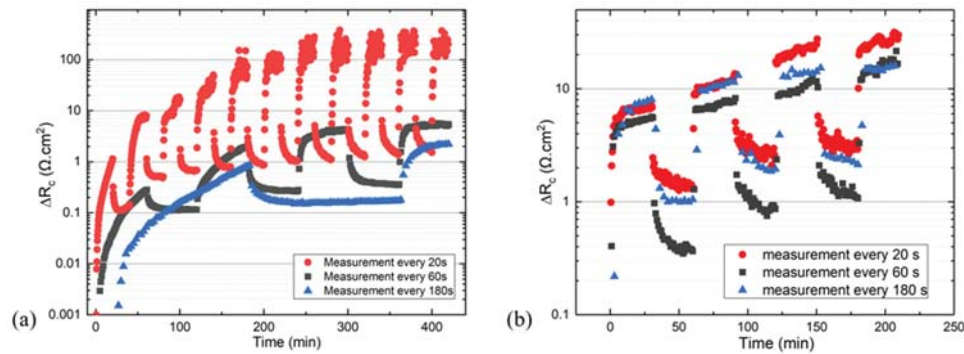


FIGURE 4. Contact resistance change with different measurement frequency. (a) ΔR_c as a function of annealing time and applied bias for a Mono PERC sample using a fixed number of measurements with a time interval of 20 s (red), 60s (gray) and 180 s (blue) at 400 °C. Since a fixed number of measurements were used, the forward and reverse bias intervals were different from each case (b) ΔR_c as a function of annealing time and applied bias for Mono PERC sample from different supplier, for the same bias duration, with measurement time interval of 20 s (grey), 60s (red) and 180 s (blue) at same time interval at 400 °C.

Influence of Pre-annealing

This and prior works indicate that the change of contact resistance during annealing appears to be related to the concentration of H, since they are controlled by bias conditions [25]. Provided that the cause of increased R_c is hydrogen passivation of interface, such ΔR_c should be proportional to the mobile hydrogen concentration in the structure. Prior work in mitigation of LeTID has used such thermal annealing to increase the H concentration available for passivation. To investigate the impact of increased H concentration on ΔR_c we tested the effect that pre-annealing conditions could have in the obtained resistance changes. FIGURE 5 (a) shows a measurement set obtained after

different pre-annealing conditions, as described in the experimental methods. Here it is clear that higher temperature pre-annealing causes faster and higher increase in ΔR_c with same applied bias. Nine samples were pre-annealed at 400 °C with different lengths of time, from 0 to 22 hours with 2.5V reverse bias before I-V characterizing for 10 minutes under 10 mA forward bias. FIGURE 5 (b) and FIGURE 5 (c) show that an increase of the pre-annealing time initially causes an increase in the rate of ΔR_c and the final saturated value of ΔR_c . However, the effect of pre-annealing saturated beyond 3 hours with the sample pre-annealed for 3 hours having the highest ΔR_c , 3.1 Ω after 70 min measurement, while ΔR_c of specimen pre-annealed 22 hours increased to around 1.5 Ω after 70 min measurement.

It is well known that Hydrogen is released from dielectric layers during firing and during subsequent rapid cooling becomes trapped in unstable forms such as hydrogen dimers [27-29]. Subsequent annealing of cells at elevated temperature can give hydrogen dimers and complexes enough time and energy to spilt into atomic hydrogen. With increasing pre-anneal temperature, more of these complexes will dissociate and the concentration of atomic hydrogen throughout the structure will increase. This is in excellent agreement with the results in Figure 5a. Pre-annealing for long times, on the other hand, led to a small subsequent decrease in the $\Delta R_c/dt$ rate. This indicates that there would still be an increased concentration of H, but to a lesser extend than for a 3 hour pre-anneal. These results show a reasonable degree of correlation between the pre-annealing conditions that lead to large rates of change of ΔR_c and thermal treatments that are effective for mitigation of LeTID [27]. Based on the difficulty of finding an LeTID treatment that does not cause HICR [17, 30], it is likely that these two effects share a common cause or are at least related.

Previous results have shown that after these thermal treatments there is greatly reduced hydrogen activity, e.g for passivation of the boron-oxygen defect [31]. This leads to two possible conclusions; the first is that during these anneals significant hydrogen effuses from the structure, leading to a greatly reduced remaining concentration. The second is that during the annealing and subsequent cooling hydrogen is able to take more stable forms, whether in the bulk or in near-surface regions. These stable forms of hydrogen do not dissociate during subsequent light soaking, and so there is no hydrogen activity either for LeTID formation or B-O passivation. The results in Figure 5b show that there is no significant decrease in the contact resistance change rate and the contact resistance change is still bias controlled after 22 hours of 400 °C pre-annealing. This is well beyond what would be needed to mitigate LeTID. If we accept a relation between mobile hydrogen concentration and HICR, this means that the concentration of mobile H in the bulk is not decreasing significantly with the long annealing durations we have shown here, in clear contradiction with the hypothesis that the majority of hydrogen has effused from the structure.

LeTID mitigation treatment therefore does not require the removal of all H from the structure, but rather that it is able to take stable forms. The importance of annealing time is then to allow sufficient thermal budget for all hydrogen present in unstable forms, which might dissociate during light soaking between 50-150°C, to first become mobile atomic hydrogen. Provided post anneal cooling is sufficiently slow the mobile hydrogen is then able to form stable complexes within the structure and play no further role in any degradation mechanisms.

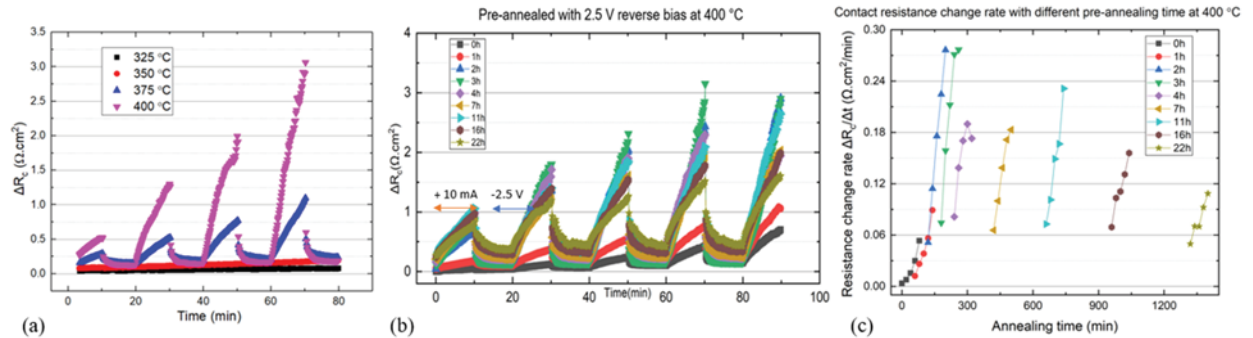


FIGURE 5. Contact resistance change with different pre-annealing conditions. (a) Contact resistance change of samples at 400 °C after 2.5 V reverse bias pre-annealing with different temperature for 2 hours. (b) Contact resistance change of samples at 400 °C after 2.5 V reverse bias pre-annealing with different pre-annealing time at 400°C. (c) Contact resistance change rate of samples at 400 °C after 2.5 V reverse bias pre-annealing with different pre-annealing time at 400°C.

CONCLUSION

In this work, we propose a modified geometry for contact resistance measurement of silicon solar cells and confirm that the increase in series resistance during post-firing annealing is solely due to contact resistance change of the front

Ag-emitter contact interface. Contact resistance is affected by the frequency of in-situ measurements and increase of measurement speed will cause the increase of contact resistance change rate. Annealing prior I-V testing increases rate of change of contact resistance. It is then possible to observe dissociation of hydrogen bound forms and subsequent behaviour of hydrogen in samples using IV measurement. We propose an explanation for how H complex dissociation during annealing and atomic hydrogen dynamics link LeTID mitigation and hydrogen induced contact resistance.

ACKNOWLEDGEMENTS

P. R. Wilshaw acknowledges support from Black Silicon Photovoltaics grant EP/R005303/1. P. Hamer acknowledges funding from the Australian Renewable Energy Agency as an ACAP fellow. R. S. Bonilla was supported by the Royal Academy of Engineering under the Research Fellowship scheme and acknowledges the support from the EPSRC Postdoctoral Fellowship EP/ M022196/1.

REFERENCES

- Schmidt, J., et al. *Impurity-related limitations of next-generation industrial silicon solar cells*. in *2012 IEEE 38th Photovoltaic Specialists Conference (PVSC) PART 2*. 2012.
- Lindroos, J. and H. Savin, *Review of light-induced degradation in crystalline silicon solar cells*. *Solar Energy Materials and Solar Cells*, 2016. **147**: p. 115-126.
- Ramspeck, K., et al., *Light Induced Degradation of Rear Passivated mc-Si Solar Cells*. Proc. 27th Eur. Photovoltaic Solar Energy Conf., 2012: p. 861-865.
- Luo, W., et al., *Potential-induced degradation in photovoltaic modules: a critical review*. *Energy & Environmental Science*, 2017. **10**(1): p. 43-68.
- Jordan, D.C. and S.R. Kurtz, *Photovoltaic Degradation Rates—an Analytical Review*. *Progress in Photovoltaics: Research and Applications*, 2013. **21**(1): p. 12-29.
- Quintana, M.A., et al. *Commonly observed degradation in field-aged photovoltaic modules*. in *Conference Record of the Twenty-Ninth IEEE Photovoltaic Specialists Conference*, 2002. 2002.
- Wohlgemuth, J.H., et al. *Assessing the causes of encapsulant delamination in PV modules*. in *2016 IEEE 43rd Photovoltaic Specialists Conference (PVSC)*. 2016.
- Bothe, K., R. Hezel, and J. Schmidt, *Recombination-enhanced formation of the metastable boron-oxygen complex in crystalline silicon*. *Applied Physics Letters*, 2003. **83**(6): p. 1125-1127.
- Hashigami, H., Y. Itakura, and T. Saitoh, *Effect of illumination conditions on Czochralski-grown silicon solar cell degradation*. *Journal of Applied Physics*, 2003. **93**(7): p. 4240-4245.
- Xi, X., et al., *Investigation of fast light-induced degradation of crystal silicon solar cells under the irradiation of a high-intensity monochromatic LED light source*. *Journal of Renewable and Sustainable Energy*, 2017. **9**(5): p. 053502.
- Kersten, F., et al., *Degradation of multicrystalline silicon solar cells and modules after illumination at elevated temperature*. *Solar Energy Materials and Solar Cells*, 2015. **142**: p. 83-86.
- Krauss, K., et al., *Light-induced Degradation of Silicon Solar Cells with Aluminiumoxide Passivated Rear Side*. *Energy Procedia*, 2015. **77**: p. 599-606.
- Zhou, C., et al., *Light and elevated temperature induced degradation in B-Ga co-doped cast mono Si PERC solar cells*. *Solar Energy Materials and Solar Cells*, 2020. **211**: p. 110508.
- Sen, C., et al., *Assessing the Impact of Thermal Profiles on the Elimination of Light- and Elevated-Temperature-Induced Degradation*. *IEEE Journal of Photovoltaics*, 2019. **9**(1): p. 40-48.
- Fung, T.H., et al., *Impact of annealing on the formation and mitigation of carrier-induced defects in multicrystalline silicon*. *Energy Procedia*, 2017. **124**: p. 726-733.
- Mäckel, H. and P. Altermatt, *Current Transport Through Lead-Borosilicate Interfacial Glass Layers at the Screen-Printed Silver-Silicon Front Contact*. Vol. 5. 2015. 1-13.
- Chan, C., et al., *Instability of Increased Contact Resistance in Silicon Solar Cells Following Post-Firing Thermal Processes*. 2017. **1**(11): p. 1700129.
- Hamer, P., et al. *The Behavior and Transport of Hydrogen in Silicon Solar Cells Observed through Changes in Contact Resistance*. in *2018 IEEE 7th World Conference on Photovoltaic Energy Conversion (WCPEC) (A Joint Conference of 45th IEEE PVSC, 28th PVSEC & 34th EU PVSEC)*. 2018.

19. Duerinckx, F. and J. Szlufcik, *Defect passivation of industrial multicrystalline solar cells based on PECVD silicon nitride*. [Solar Energy Materials and Solar Cells](#), 2002. **72**(1): p. 231-246.
20. Martinuzzi, S., I. Périchaud, and F. Warchol, *Hydrogen passivation of defects in multicrystalline silicon solar cells*. [Solar Energy Materials and Solar Cells](#), 2003. **80**(3): p. 343-353.
21. Hoex, B., et al., *Silicon surface passivation by atomic layer deposited Al₂O₃*. [Journal of Applied Physics](#), 2008. **104**(4): p. 044903.
22. Dingemans, G., et al., *Influence of annealing and Al₂O₃ properties on the hydrogen-induced passivation of the Si/SiO₂ interface*. [Journal of Applied Physics](#), 2012. **111**(9): p. 093713.
23. Kersten, F., J. Heitmann, and J. Mueller, *Influence of Al₂O₃ and SiN_x passivation layers on LeTID*. [Energy Procedia](#), 2016. **92**: p. 828-832.
24. Vargas, C., et al., *Carrier-Induced Degradation in Multicrystalline Silicon: Dependence on the Silicon Nitride Passivation Layer and Hydrogen Released During Firing*. [IEEE Journal of Photovoltaics](#), 2018. **8**(2): p. 413-420.
25. Hamer, P., et al., *Hydrogen induced contact resistance in PERC solar cells*. [Solar Energy Materials and Solar Cells](#), 2018. **184**: p. 91-97.
26. Sen, C., et al. *Different Extent and Behaviour of LeTID in the Past and Current PERC Silicon Solar Cells*. in *Asia-Pacific Solar Research Conference*. 2019.
27. Yli-Koski, M., et al., *Low-temperature dark anneal as pre-treatment for LeTID in multicrystalline silicon*. [Solar Energy Materials and Solar Cells](#), 2019. **192**: p. 134-139.
28. Sen, C., et al., *Eliminating light- and elevated temperature-induced degradation in P-type PERC solar cells by a two-step thermal process*. [Solar Energy Materials and Solar Cells](#), 2020. **209**: p. 110470.
29. Pritchard, R.E., et al., *Hydrogen molecules in boron-doped crystalline silicon*. [Semiconductor Science and Technology](#), 1999. **14**(1): p. 77-80.
30. Peral, A., et al., *Impact of Extended Contact Cofiring on Multicrystalline Silicon Solar Cell Parameters*. [IEEE Journal of Photovoltaics](#), 2017. **7**(1): p. 91-96.
31. Kim, M., et al., *Role of hydrogen: Formation and passivation of meta-stable defects due to hydrogen in silicon*. [AIP Conference Proceedings](#), 2018. **1999**(1): p. 130010.